Electrochemical Analysis of Changes in Iron Oxide Reducibility during Abiotic Ferrihydrite Transformation into Goethite and Magnetite

Meret Aeppli,[†,‡] Ralf Kaegi,[‡] Ruben Kretzschmar,[†] Andreas Voegelin,[‡] Thomas B. Hofstetter,*[,†,‡] and Michael Sander*[,†]

†Institute of Biogeochemistry and Pollutant Dynamics, ETH Zürich, 8092 Zürich, Switzerland

‡Swiss Federal Institute of Aquatic Science and Technology (Eawag), 8600 Dübendorf, Switzerland

Ⓢ *Supporting Information*

ABSTRACT: Electron transfer to ferric iron in (oxyhydr-) oxides (hereafter iron oxides) is a critical step in many processes that are central to the biogeochemical cycling of elements and to pollutant dynamics. Understanding these processes requires analytical approaches that allow for characterizing the reactivity of iron oxides toward reduction under controlled thermodynamic boundary conditions. Here, we used mediated electrochemical reduction (MER) to follow changes in iron oxide reduction extents and rates during abiotic ferrous iron-induced transformation of six-line ferrihydrite. Transformation experiments (10 mM ferrihydrite-Fe^{III}) were conducted over a range of solution conditions (pH$_{trans}$ = 6.50 to 7.50 at 5 mM Fe^{2+} and for pH$_{trans}$ = 7.00 also

at 1 mM Fe^{2+}) that resulted in the transformation of ferrihydrite into thermodynamically more stable goethite or magnetite. The changes in iron oxide mineralogy during the transformations were quantified using X-ray diffraction analysis. MER measurements on iron oxide suspension aliquots collected during the transformations were performed over a range of pH$_{MER}$ at constant applied reduction potential. The extents and rates of iron oxide reduction in MER decreased with decreasing reaction driving force resulting from both increasing pH$_{MER}$ and increasing transformation of ferrihydrite into thermodynamically more stable iron oxides. We show that the decreases in iron oxide reduction extents and rates during ferrihydrite transformations can be linked to the concurrent changes in iron oxide mineralogy.
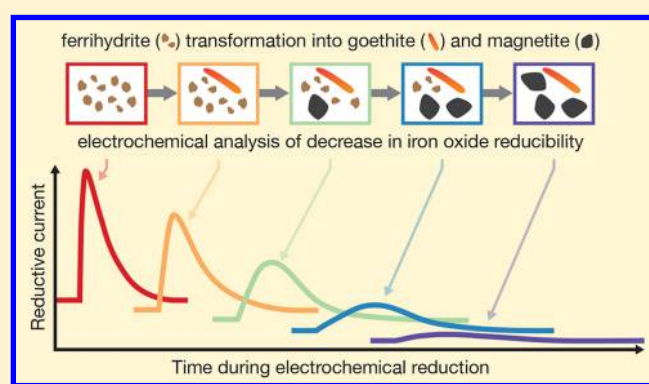
INTRODUCTION

Electron transfer to ferric iron (Fe^{III}) in iron (oxyhydr-)oxides (hereafter referred to as iron oxides) plays a key role in numerous processes that control the biogeochemical cycling of nutrients and trace metals as well as the dynamics of organic and inorganic pollutants in both natural and engineered systems.[1−3] Electrons are transferred to Fe^{III} abiotically from chemical reductants, such as reduced natural organic matter[4,5] and reduced sulfur species,[6,7] as well as biotically in the presence of iron-reducing bacteria and archaea.[8−10] While electron transfer reactions involving iron oxides occur with various reductants and under very different environmental and experimental conditions, all of these redox reactions critically depend of the reactivity of the iron oxide toward accepting electrons. We refer to this reactivity as iron oxide reducibility, which we define to include both rates and extents of oxide-Fe^{III} reduction. As a consequence, there is considerable interest in various research areas in analytical approaches that allow for characterizing iron oxide reducibility.

A prerequisite for analytical approaches to assess iron oxide reducibility is an accurate control of the thermodynamic

boundary conditions for iron oxide reduction. These conditions depend on the properties of the iron oxide(s) in the sample of interest. Arguably the most important properties are the mineralogy and crystallinity of the iron oxide because they define its thermodynamic stability. Short-range ordered iron oxides, such as ferrihydrite, have lower thermodynamic stabilities (and higher solubilities[11]) than long-range ordered iron oxides, such as goethite, hematite, and magnetite. These stability differences are reflected in the higher reduction potential of ferrihydrite (E_H(oxide) = +0.012 V at pH 7[12]) than of goethite, hematite, and magnetite (E_H(oxide) = −0.277, −0.286, −0.310 V, respectively, at pH 7[12]). Because iron oxide reduction is a heterogeneous reaction, the iron oxide surface area and aggregation state as well as possible surface adsorbates will modulate the reducibility of the iron oxide.[13,14] Besides iron oxide properties, the thermodynamics of iron
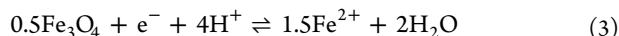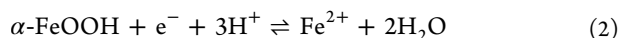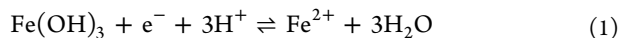
oxide reduction also depend on solution pH, ferrous iron (Fe^{2+}) concentration, and the reduction potential of the reductant ($E_H(reductant)$). Because electron transfer to iron oxides is coupled to proton transfer, as shown for the reductive dissolution of ferrihydrite (denoted for simplicity as Fe-$(OH)_3$), goethite (α-FeOOH), and stoichiometric magnetite (Fe_3O_4) in eqs 1−3, increasing solution pH lowers the feasibility of iron oxide reduction (i.e., the reaction driving force, $\Delta_r G$, increases toward less negative values).

$$Fe(OH)_3 + e^- + 3H^+ \rightleftharpoons Fe^{2+} + 3H_2O \quad (1)$$

$$\alpha\text{-FeOOH} + e^- + 3H^+ \rightleftharpoons Fe^{2+} + 2H_2O \quad (2)$$

$$0.5Fe_3O_4 + e^- + 4H^+ \rightleftharpoons 1.5Fe^{2+} + 2H_2O \quad (3)$$

Similarly, increasing $E_H(reductant)$ in the analysis shifts $\Delta_r G$ to less favourable values. The combined effects of $E_H(oxide)$, $E_H(reductant)$, and solution pH on $\Delta_r G$ are described in eq 4:

$$\Delta_r G = -n \cdot F \cdot (E_H(oxide) - E_H(reductant))$$

$$= -n \cdot F \cdot \left(E_H^0(oxide) - \frac{R \cdot T}{n_{e^-} \cdot F} \cdot 2.303 \cdot \right.$$

$$\left. (m_{Fe^{2+}} \cdot \log(\{Fe^{2+}\}) + m_{H^+} \cdot pH) - E_H(reductant) \right)$$

$$(4)$$

where F is the Faraday constant, R is the gas constant, T is the absolute temperature, n is the number of electrons transferred in the overall reaction, $E_H^0(oxide)$ is the standard reduction potential of the iron oxide, $\{Fe^{2+}\}$ is the activity of aqueous ferrous iron (which increases if the oxide undergoes reductive dissolution), and n_{e^-}, m_{H^+} and $m_{Fe^{2+}}$ denote the stoichiometric coefficients for e^-, H^+ and Fe^{2+}, respectively, in the reductive iron oxide dissolutions shown in eqs 1−3.

Analytical approaches to characterize iron oxide reducibility may thus use solution pH and $E_H(reductant)$ as adjustable parameters to adapt $\Delta_r G$. Existing wet chemistry approaches, however, provide only limited capability to control and adjust these parameters. These approaches rely on reacting iron oxides with chemical reductants while monitoring changes in the concentrations of Fe^{2+} or the chemical reductant.[15−19] While these analyses can, in principle, be conducted at different solution pH, most of the used chemical reductants undergo proton-coupled electron transfers and thus have pH-dependent $E_H(reductant)$. As a consequence, solution pH and $E_H(reductant)$ cannot be independently altered in these approaches. Furthermore, electron transfer from the reductant to iron oxides increases the $E_H(reductant)$, and thus continuously shifts $\Delta_r G$ to less favorable values as the redox reaction progresses.

We recently showed that these limitations inherent to wet chemistry approaches can be overcome by mediated electrochemical reduction (MER).[20−22] In this approach, a suspended iron oxide is transferred into an electrochemical cell in which the working electrode (WE) is polarized to defined and constant reduction potential, E_H^{MER}. The cell contains a dissolved, one-electron transfer mediator (i.e., the reductant) in redox equilibrium with the WE (i.e., $E_H(reductant) = E_H^{MER}$). Because electron transfer to and from the mediator is not coupled to proton transfer, the mediator redox speciation and thus also $E_H(reductant)$ remain unaffected by altering the solution pH in the electrochemical cell (pH_{MER}). Electron

transfer from the WE via the mediator to oxide-Fe^{III} results in reductive current peaks that can be analyzed both for the total number of transferred electrons (by peak integration) and the rates of electron transfer (by analysis of peak height and shape). In our previous work,[20] we demonstrated that MER can be used to quantify differences in the reduction extents and rates of ferrihydrite, goethite and hematite at varying pH_{MER} and E_H^{MER} and thus over a range of thermodynamic boundary conditions for reduction. The analyses showed that the reducibilities of these oxides increased as the $\Delta_r G$ became increasingly exergonic. Yet, in our previous work, we limited the analyses to suspensions that contained only a single iron oxide that did not transform over time.

The goal of this work was to demonstrate the analytical capability of MER to characterize changes in iron oxide reducibility in samples containing more than one iron oxide and to assess whether the changes in reducibility can be directly linked to changes in iron oxide mineralogy. Demonstrating this analytical capability is a critical step toward establishing that MER can be applied to complex iron oxide-containing samples collected from laboratory incubations or field systems. As a model system to achieve our goal, we chose the well-studied abiotic ferrous iron-induced transformation of six-line ferrihydrite into goethite and magnetite with distinct changes in iron oxide mineralogy as a function of solution pH and Fe^{2+} concentration.[23−39] It is challenging to measure changes in the reducibilities of iron oxide suspension aliquots collected over the course of these transformations because they may contain mixtures of ferrihydrite, goethite and magnetite and thus iron oxides with different reducibilities. Assessing iron oxide reducibility in these samples thus requires analyses over a wide range of thermodynamic boundary conditions for iron oxide reduction. We accomplished this by analyzing samples at $pH_{MER} = 5.00$ to 7.25, all at constant $E_H^{MER} = -0.35$ V. We complemented the MER analysis of iron oxide suspension aliquots by X-ray diffraction (XRD) and electron microscopy (EM) analyses to determine the mineralogy of the iron oxides. These combined analyses served to assess whether changes in iron oxide reducibility determined by MER over the course of the ferrihydrite transformations can be directly linked to the underlying mineralogical changes.

■ MATERIALS AND METHODS

Solutions and Suspensions. All solutions and mineral suspensions were prepared with doubly deionized water (DDW, resistivity >18.2 MΩ·cm, Barnstead Nanopure Diamond Water Purification System) and were made anoxic by purging them with ultrahigh purity N_2 for at least 3 h prior to transfer into an anoxic glovebox (see below).[20] Solutions for MER measurements contained 0.01 M KCl as electrolyte and 0.01 M organic pH buffers (i.e., acetic acid ($pK_a = 4.75$) for measurements at $pH_{MER} = 5.00$ to 5.50; 2-(N-morpholino)-ethanesulfonic acid (MES; $pK_a = 6.15$) at $pH_{MER} = 6.00$ to 6.50; 3-morpholinopropane-1-sulfonic acid (MOPS; $pK_a = 7.2$) at $pH_{MER} = 6.75$ to 7.25). Section S1 in the Supporting Information lists all chemicals used.

Ferrihydrite Transformation Experiments. Ferrihydrite transformation experiments were run at $pH_{trans} = 6.50$ to 7.50 with initial Fe^{2+} concentrations of 5 mM, and at $pH_{trans} = 7.00$ also with 1 mM Fe^{2+} (all at 10 mM ferrihydrite-Fe^{III}). We selected these conditions based on past studies[23−39] to result in ferrihydrite transformation into goethite (low Fe^{2+}), magnetite

(high pH_{trans} and Fe^{2+}), and goethite−magnetite mixtures (intermediate pH_{trans}).

Transformation experiments, sample preparation for XRD and EM analyses, as well as MER measurements were performed inside an anoxic glovebox (N_2 atmosphere, < 2 ppm O_2; Unilab 2000, MBraun). An overview of the experimental setup, sample preparation, and analysis is provided in Section S2. Six-line ferrihydrite was synthesized according to Schwertmann and Cornell[40] (Section S3) and used in the transformation experiments within 1 week of being synthesized. Transformations were run in duplicates at each solution condition in 1L high-density polyethylene bottles under continuous stirring (400 rpm, overhead stirrers) with initial Fe^{III} concentrations in ferrihydrite of 10 mM (solution volume: 400 mL). Proton release into solution resulting from the mineralogical transformations was detected by pH-stat titration and was compensated for by automated titration of 70 mM KOH (907 Titrando, Metrohm). We chose this KOH concentration because it was high enough to minimize dilution of the suspension by base addition but low enough to avoid overdosing. The resulting pH-stat titration curves and added base volumes are shown in Section S4.

At selected transformation time points, we collected 7.0 mL suspension aliquots from the reactors. On these aliquots, we determined iron oxide mineralogy by XRD and EM analyses and characterized iron oxide reducibility by MER (see below). We note that in the experiments at pH_{trans} = 7.00, 7.25, and 7.50, transformations were too rapid to allow for parallel MER analyses of aliquots collected from both duplicate reactors at intermediate time points during the experiments. In these cases, we only analyzed aliquots collected from one of the duplicate reactors by MER. A Fe^{2+}-free control experiment containing only 10 mM ferrihydrite-Fe^{III} showed no transformation of ferrihydrite over 600 h (at pH_{trans} = 7.00, Section S5). After each transformation experiment was terminated, we used the phenanthroline assay[41] to quantify total Fe and Fe^{2+} concentrations in both unfiltered suspension aliquots and solutions obtained by filtration (0.22 μm syringe filters, Section S6). We freeze-dried the remaining suspensions and determined the specific surface areas of the resulting iron oxide powders by N_2−BET measurements (Nova 3200e, Quantachrome, Section S7).

X-ray Diffraction Analysis of Iron Oxides. For XRD analysis, 4.5 mL of each 7.0 mL suspension aliquot (see above) were washed by sequential centrifugation (1−14 Microfuge, Sigma), removal of the supernatant, and resuspension of the resulting pellet in DDW. This procedure was repeated twice before finally resuspending the pellet in ethanol, followed by depositing the suspension onto a zero background Si(510) slide (Siltronix) and drying the deposited sample in a desiccator inside the glovebox. For analysis, the slide was placed into an airtight specimen holder with a dome-like X-ray transparent cap (Bruker AXS) and sealed airtight in the anoxic glovebox before being transferred to the XRD instrument (D8 Advance, Bruker). X-ray diffractograms were recorded from 10 to 70°2θ (step size 0.02°2θ, 10 s acquisition time per step) in Bragg−Brentano geometry using Cu Kα radiation (λ = 1.5418 Å, 40 kV, and 40 mA) and a high-resolution energy dispersive 1-D detector (LYNXEYE).

Iron oxide mass fractions in the samples were quantified by Rietveld quantitative phase analysis of the diffractograms as detailed in Section S8. For the analysis, we used published structure files for magnetite, goethite, lepidocrocite, and siderite (Inorganic Crystal Structure Database, FIZ Karlsruhe) and calibrated ferrihydrite as hkl phase using the partial or no known crystal structure (PONKCS) approach.[42,43] We verified accurate quantification of ferrihydrite mass fractions with the PONKCS approach by analyzing ferrihydrite−goethite and ferrihydrite−magnetite mixtures that we prepared to have different mass fractions of the two respective minerals. In Rietveld fitting of sample diffractograms, we only included iron oxides that showed characteristic peaks in the diffractograms. Preferred orientation of goethite (100, 110) and lepidocrocite (010) was considered in Rietveld fitting (March Dollase method, TOPAS). Iron oxide mass fractions were converted into molar fractions of Fe^{III} using the molar mass of each iron oxide. We estimated magnetite stoichiometry based on the unit-cell length of magnetite[44] and determined pseudo-first order rate constants for ferrihydrite transformation into goethite and magnetite.

Electron Microscopy. For EM investigations, 0.5 mL of each 7.0 mL suspension aliquot (see above) was washed by sequential centrifugation (1−14 Microfuge, Sigma), removal of the supernatant, and resuspension of the resulting pellet in DDW. This washing step was repeated once before the pellet was resuspended in DDW and drop-deposited onto a grid coated with a holey carbon support film. All grids were stored in the glovebox and transported outside the glovebox in a vacuum desiccator. The grids were analyzed using a dedicated scanning transmission electron microscope (STEM, 2700Cs, Hitachi) operated at an acceleration voltage of 200 kV. For image acquisition, either a secondary electron or a high angular annular dark field detector was used.

Characterization of Iron Oxide Reducibility by MER. We determined the extents and rates of iron oxide reduction in each 7.0 mL suspension aliquot (see above) by MER following procedures introduced recently.[20,21] MER measurements were performed over a wide range of $\Delta_r G$ for iron oxide reductive dissolution by varying pH_{MER} among electrochemical cells in increments of 0.50 pH units from pH_{MER} = 5.00 to 6.00 and in increments of 0.25 pH units from pH_{MER} = 6.00 to 7.25, all at constant E_H^{MER} = −0.35 V. These variations in pH_{MER} resulted in increases in $\Delta_r G$ for ferrihydrite reductive dissolution from −70 kJ $mol^{-1}_{e^- \text{ transferred}}$ at pH_{MER} = 5.00 to −32 kJ $mol^{-1}_{e^- \text{ transferred}}$ at pH_{MER} = 7.25, and increases in $\Delta_r G$ for goethite and magnetite reductive dissolution from −50 and −56 kJ $mol^{-1}_{e^- \text{ transferred}}$, respectively, at pH_{MER} = 5.00 to −11 and −4.2 $mol^{-1}_{e^- \text{ transferred}}$ at pH_{MER} = 7.25 (Section S9).

Electrochemical cells were controlled by two eight-channel potentiostats (models 1000B and 1000C, CH Instruments) operated in amperometric i-t curve mode. We used glassy carbon working electrode (WE) cylinders (9 mL, GAZ 1, HTW) to hold the reaction solutions, which were continuously stirred by Teflon-coated stir bars using stir plates positioned below the cells (MIXdrive 1 XS, 2mag). Platinum wires separated from the WE compartment by glass frits (PORE E tubes, ACE glass) served as counter electrodes. We used Ag/AgCl reference electrodes (Re1B, ALS) but herein report E_H^{MER} values versus the standard hydrogen electrode.

MER measurements were performed as follows (an exemplary current response is shown in Section S10). The WE cylinder was filled with 5.22 mL of a solution buffered to a defined pH_{MER} (see above) and the measurement was initiated by applying a constant E_H^{MER} = −0.35 V to the WE. After attainment of a stable baseline current, we added the electron transfer mediator diquat (1,1′-ethylene-2,2′-bipyridyl, standard
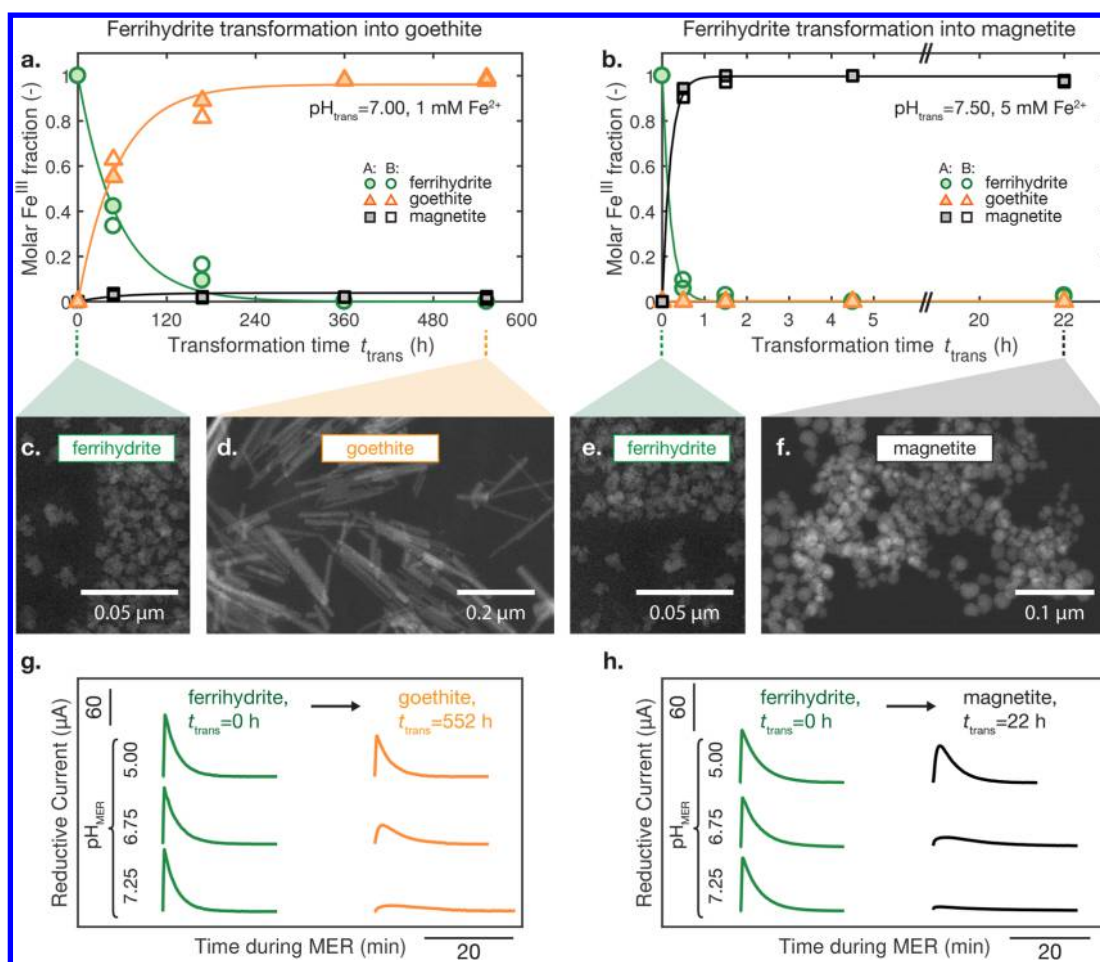
Figure 1. Changes in iron oxide mineralogy, morphology and reducibility during ferrihydrite transformation into goethite (pH_{trans} = 7.00, 1 mM Fe^{2+}, 10 mM ferrihydrite-Fe^{III}) and magnetite (pH_{trans} = 7.50, 5 mM Fe^{2+}, 10 mM ferrihydrite-Fe^{III}). (a, b) Changes in the molar fractions of Fe^{III} in ferrihydrite, goethite, and magnetite over the course of the transformations as determined using X-ray diffraction analysis. Molar Fe^{III} fractions are shown separately for duplicate reactors (reactors A and B in filled and open symbols, respectively) and were determined from the iron oxide mass fractions as described in Section S8.5. The mass fractions of crystalline siderite and lepidocrocite were <1.2% in all samples. Solid lines depict fitting of eqs S6−S8 to the concentrations of Fe^{III} in ferrihydrite, goethite, and magnetite (Section S8.7). (c−f) Transmission electron microscopy images of initial ferrihydrite and resulting goethite and magnetite. (g, h) Exemplary reductive current responses during mediated electrochemical reduction (MER) at pH_{MER} = 5.00, 6.75, and 7.25 (all at applied reduction potentials of E_H^{MER} = −0.35 V) of iron oxide suspensions collected from the reactors at the beginning and the end of the transformations.

reduction potential E_H^0 = −0.35 V,[45] which equaled E_H^{MER}) to the electrochemical cell from a 10 mM stock solution in three separate additions. All diquat additions resulted in a reductive current peak. The first addition had a large volume and resulted in a diquat concentration in the WE cylinder of 0.436 mM. The subsequent two mediator additions had smaller, identical volumes that each increased the mediator concentration by 0.036 mM. These smaller mediator additions enabled us to characterize slight differences in the responsiveness of the electrochemical cells to the addition of oxidized mediator or iron oxides. We corrected maximum rates of iron oxide reduction for these differences, as detailed below. Following reattainment of a stable background current after the last mediator addition, 20 μL of the 7.0 mL aliquots collected during the transformation experiments were added to the MER cell. Electron transfer from reduced diquat to the added oxide-Fe^{III} resulted in a reductive current peak as the response of the system to maintaining constant E_H^{MER} during the analysis. We terminated the MER measurement upon return of the reductive current to background values.

We determined the moles of electrons transferred from the WE to the iron oxide and thus the number of Fe^{III} atoms reduced, Fe_{MER}^{III} ($mol_{Fe^{III}}$), by integration of the reductive current peak (eq S[45]):

$$Fe_{MER}^{III} = \frac{1}{F} \int_{t_0}^{t_{end}} I(t) \, dt \tag{5}$$

where $I(t)$ (A) is the baseline-corrected reductive current, and t_0 and t_{end} (s) denote the initial (i.e., the time of oxide addition) and final (i.e., the time at which background currents were reattained) integration boundaries of the reductive current peak. Baseline subtraction and peak integration were performed using Matlab (MathWorks) (code in Section S11). We report Fe_{MER}^{III} as a fraction of the total number of Fe^{III} atoms in the analyzed sample (Fe_{total}^{III}). The latter was determined by MER measurements at low pH_{MER} = 5.00, 5.50, and 6.00. Under these conditions, $\Delta_r G$ was sufficiently negative to result in complete reduction of oxide-Fe^{III} irrespective of iron oxide mineralogy. Complete reduction was confirmed by agreement of Fe_{MER}^{III} measured in MER with

the total number of Fe^{III} atoms determined using the phenanthroline assay (Figure S8).

The reductive current in MER is a direct measure of the rate at which electrons are transferred from the WE to redox-active species in solution. Herein, we report iron oxide reduction rates in terms of the maximum current, I_{max}^{oxide} (i.e., maximum height of iron oxide peak) according to eq 6:

$$r_{max}^{norm} = \frac{1}{F} \cdot I_{max}^{oxide} \cdot \left(\frac{I_{max}^{med,av}}{I_{max}^{med}} \right) \cdot \left(\frac{1}{Fe_{total}^{III}} \right) \tag{6}$$

where r_{max}^{norm} ($mol_{e^-} \; mol_{Fe^{III}}^{-1} \; s^{-1}$) is the normalized maximum reduction rate, I_{max}^{oxide} and I_{max}^{med} are the maximum reductive currents in response to iron oxide and mediator additions to the electrochemical cells, respectively, and $I_{max}^{med, av} = 39.2 \; \mu A$ is the mediator I_{max} averaged over all MER measurements. I_{max} values were determined as detailed in Section S11. The term $(I_{max}^{med, av}/I_{max}^{med})$ corrects for small differences in the responsiveness among individual electrochemical cells.[20] We normalized I_{max}^{oxide} to Fe_{total}^{III} to account for the fact that decreasing amounts of Fe_{total}^{III} were added to the MER cells over the course of the transformations due to the dilution of iron oxide suspensions by base titration during the transformation experiments. Note that we describe iron oxide reduction rates by r_{max}^{norm} instead of reduction rate constants as used previously[20] because the former allowed us to quantify rates also in MER measurements in which iron oxide reduction was incomplete. Furthermore, at the time when I_{max}^{oxide} was reached, only a small fraction of the iron oxide has been reduced and hence the probability for iron oxide phase transformation during MER was low.

■ RESULTS AND DISCUSSION

Changes in Iron Oxide Reducibility during Ferrihydrite Transformation into Goethite or Magnetite. *MER of Ferrihydrite and Its Transformation End-Products Goethite and Magnetite.* We first ran duplicate ferrihydrite transformation experiments (10 mM initial ferrihydrite-Fe^{III}) at two solution conditions that we selected based on past studies to result in the formation of either goethite (i.e., $pH_{trans} = 7.00$ and 1 mM Fe^{2+}) or magnetite (i.e., $pH_{trans} = 7.50$ and 5 mM Fe^{2+}). Figure 1a and b show the temporal changes in the molar fractions of Fe^{III} in ferrihydrite, goethite, and magnetite during these experiments, as determined by XRD on suspension aliquots collected over the course of the transformations. Crystalline siderite and lepidocrocite were formed in only very small amounts (mass fractions <1.2%). At $pH_{trans} = 7.00$ and 1 mM Fe^{2+} (Figure 1a), ferrihydrite transformed into goethite over approximately one month with a pseudo-first order rate constant $k_{FH \rightarrow GOE}$ of $(17.8 \pm 2.10) \cdot 10^{-3}$ h^{-1} (fits shown as solid lines in panel a; the fitting procedure is described in Section S8.7). Conversely, at $pH_{trans} = 7.50$ and 5 mM Fe^{2+}, ferrihydrite transformed into magnetite within only 1.5 h of Fe^{2+} addition with a $k_{FH \rightarrow MAG}$ of (5.16 ± 0.32) h^{-1} (Figure 1b). The formed magnetite was nonstoichiometric with a molar ratio of structural $Fe^{III}:Fe^{II}$ of 1:0.4, as determined from X-ray diffractograms of magnetite[44] (Section S8.6). Proton release into solution was small when ferrihydrite transformed into goethite (<0.1 mol H^+ released per mol Fe^{III}) but large when ferrihydrite transformed into magnetite (~0.9 mol H^+ released per mol Fe^{III}), consistent with the stoichiometries of the two transformation reactions (Section S12). Electron microscopy images show that ferrihydrite was present as aggregated primary crystallites with sizes of a few nm (Figure

1c,e). Transformation of ferrihydrite resulted in the formation of needle-shaped goethite with widths ranging from 10 to 70 nm and lengths ranging from 200 to 400 nm (Figure 1d) and close to spherical magnetite with diameters ranging from 10 to 30 nm (Figure 1f). Additional EM images collected over the course of the transformations are shown in Figures S23 and S28.

We characterized the reducibilities of ferrihydrite and its transformation products goethite and magnetite by MER over a range of pH_{MER} from 5.00 to 7.25 (all at $E_H^{MER} = -0.35$ V). Figure 1g and h show selected reductive current peaks of ferrihydrite (green traces), goethite (orange traces), and magnetite (black traces) determined at three of the tested pH_{MER} (i.e., $pH_{MER} = 5.00$, 6.75, and 7.25). Ferrihydrite addition to MER cells resulted in sharp reductive current peaks at all tested pH_{MER}, demonstrating that ferrihydrite was readily reduced under all MER conditions. By comparison, the reductive current peaks of goethite and magnetite decreased in height and increased in widths with increasing pH_{MER}. The reducibility of goethite and magnetite therefore decreased (in terms of both reduction rates and extents, as detailed below) as the thermodynamic feasibility of electron transfer to these oxides decreased.

To express differences in the reducibilities of ferrihydrite, goethite, and magnetite in quantitative terms, we determined both their reduction extents (by peak integration, eq 5) and maximum reduction rates (from peak maxima, eq 6) from their reductive current peaks in MER. Figure 2a and b show the effect of pH_{MER} on the fractions of total Fe^{III} in ferrihydrite, goethite, and magnetite that were reduced in MER (i.e., $Fe_{MER}^{III}/Fe_{total}^{III}$). MER of ferrihydrite resulted in $Fe_{MER}^{III}/Fe_{total}^{III}$ of unity at all pH_{MER}, which implied that ferrihydrite underwent complete reductive dissolution at all tested pH_{MER}. The thermodynamics of ferrihydrite reduction were therefore sufficiently favorable even at the highest tested pH_{MER} of 7.25 to result in complete ferrihydrite reduction. In contrast to ferrihydrite, goethite and magnetite were completely reduced in MER only at low $pH_{MER} \leq 7.00$ and 6.25, respectively (Figure 2a,b). At pH_{MER} above these values, $Fe_{MER}^{III}/Fe_{total}^{III}$ decreased with increasing pH_{MER} to values of 0.72 ± 0.06 for goethite and 0.38 ± 0.03 for magnetite at the highest tested pH_{MER} of 7.25. Goethite and magnetite reduction therefore became increasingly incomplete as the thermodynamic feasibility of electron transfer to these oxides decreased. We note that part of the reductive current responses of magnetite at $pH_{MER} > 6.25$ may have involved electron transfer to structural Fe^{III} to form stoichiometric magnetite. We estimated that this electron transfer contributed at most $Fe_{MER}^{III}/Fe_{total}^{III} = 0.06$ based on the stoichiometry of the analyzed magnetite.

Comparable to its effects on reduction extents, pH_{MER} also had a much smaller effect on the normalized maximum reduction rates (i.e., r_{max}^{norm}; eq 6) of ferrihydrite than of goethite and magnetite. We chose to present normalized instead of absolute maximum rates to account for small differences in the responsiveness among individual MER cells (see Materials and Methods). The r_{max}^{norm} values of ferrihydrite were high over the entire pH_{MER} range with only a small step decrease from $pH_{MER} = 6.25$ to 7.00. We note that these high rates may have been controlled, in part, by the reduction of the mediator and that ferrihydrite reduction rates may have been even higher.[20] In contrast to ferrihydrite, r_{max}^{norm} of both goethite and magnetite decreased with increasing $pH_{MER} > 6.25$ and 5.00, respectively. At the highest $pH_{MER} = 7.25$, the r_{max}^{norm} were approximately five-
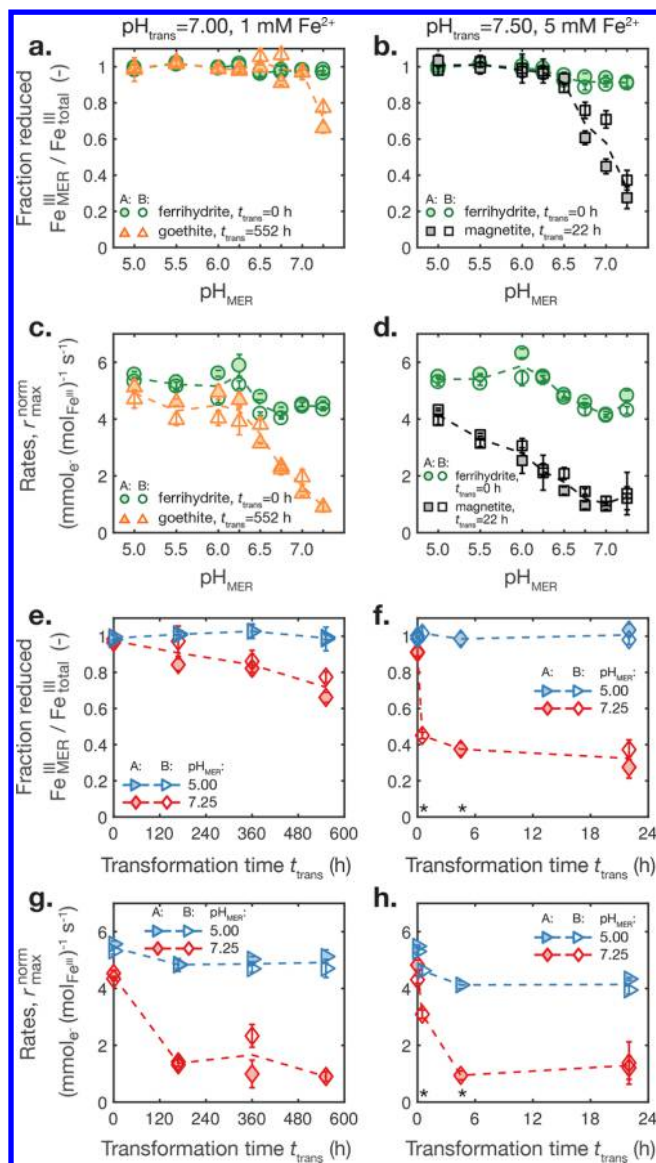
Figure 2. Changes in iron oxide reducibility during ferrihydrite transformation into goethite and magnetite as assessed using mediated electrochemical reduction (MER) at pH_{MER} = 5.00 to 7.25, all at applied reduction potentials of E_H^{MER} = −0.35 V. MER measurements were performed on iron oxide suspension aliquots collected from duplicate reactors (reactors A and B in filled and open symbols, respectively). Fractions of oxide-Fe^{III} reduced (Fe_{MER}^{III}/Fe_{total}^{III}) are shown versus (a, b) pH_{MER} and (e, f) transformation time. We note that for the transformation experiment at pH_{trans} = 7.5, MER data were collected for only one of the duplicate reactors at transformation times of 0.5 h (reactor B) and 4.5 h (reactor A) (marked with ∗ on the x axes) because the transformation progressed too rapidly to allow for parallel MER analyses of aliquots collected from both reactors. Normalized maximum iron oxide reduction rates (r_{max}^{norm}) are shown versus (c, d) pH_{MER} and (g, h) transformation time. Fe_{MER}^{III}/Fe_{total}^{III} and r_{max}^{norm} were determined as described in the Materials and Methods section. Dashed lines in all panels serve as visual guides.

and three-fold smaller than those measured for goethite and magnetite, respectively, at the lowest pH_{MER} of 5.00. A comparison of panels a,b and c,d of Figure 2 shows that for both goethite and magnetite, r_{max}^{norm} started to decrease at lower pH_{MER} and showed larger relative decreases as compared to Fe_{MER}^{III}/Fe_{total}^{III} of the same iron oxides. Reduction rates were

therefore more sensitive than reduction extents to changes in pH_{MER} and thus to changes in the thermodynamic boundary conditions for reduction. The finding that r_{max}^{norm} decreased over a wider pH_{MER} range for magnetite than for goethite likely reflected the stronger pH-dependence of the E_H(oxide) of magnetite than goethite (i.e., transfers of 4 versus 3 protons per electron transferred for magnetite (eq 3) and goethite (eq 2), respectively).

In conclusion, the differences in the effects of pH_{MER} on the extents and maximum rates of ferrihydrite, goethite and magnetite reduction are consistent with the lower thermodynamic stability of poorly crystalline ferrihydrite than of its crystalline transformation products goethite and magnetite (Section S9). MER can reveal these differences in the reducibilities among the three iron oxides and changes in these reducibilities with pH_{MER}. Furthermore, the pronounced differences in the reducibilities of ferrihydrite and its transformation products goethite and magnetite, particularly at high pH_{MER}, suggest that MER can be employed not only to characterize the reducibilities of the transformation end-products, but also of iron oxide mixtures collected over the course of the transformations.

MER of Ferrihydrite−Goethite and Ferrihydrite−Magnetite Mixtures during Ferrihydrite Transformations. Figure 2 shows the changes in the extents (panels e, f) and maximum rates (panels g, h) of iron oxide reduction in MER for samples collected over the course of the ferrihydrite transformations into goethite or magnetite (mineralogical changes shown in Figure 1a,b). We plotted only the MER data obtained at the lowest and highest pH_{MER} = 5.00 and 7.25, which corresponded to the most and least thermodynamically favorable conditions for iron oxide reduction, respectively. Reduction extents and rates at intermediate pH_{MER} lay in between the values measured at the lowest and highest pH_{MER} (Section S14).

MER at pH_{MER} = 5.00 resulted in complete reductive dissolution of all ferrihydrite−goethite and ferrihydrite−magnetite mixtures that were collected over the course of the ferrihydrite transformations (i.e., Fe_{MER}^{III}/Fe_{total}^{III} of ≈ 1, Figure 2e,f). Similarly, the maximum reduction rates of the iron oxide mixtures at pH_{MER} = 5.00 decreased only slightly with increasing transformation of ferrihydrite into goethite (Figure 2g) or magnetite (Figure 2h). Conversely, MER analyses of the same ferrihydrite−goethite and ferrihydrite−magnetite mixtures at the highest pH_{MER} = 7.25 revealed that both extents and maximum rates of iron oxide reduction decreased with increasing transformation of ferrihydrite into goethite (Figure 2e,g) or magnetite (Figure 2f,h). As argued above, the lower reducibility of these samples at pH_{MER} = 7.25 compared to 5.00 reflected the smaller thermodynamic driving force for iron oxide reductive dissolution at the higher pH_{MER}. The decrease in iron oxide reducibility at pH_{MER} = 7.25 over the course of the transformations can thus be ascribed to decreasing concentrations of the metastable, poorly crystalline ferrihydrite and increasing concentrations of the more stable, crystalline goethite and magnetite in the mixtures. Finally, the more rapid and extensive decrease in the reduction extents at pH_{MER} = 7.25 for ferrihydrite−magnetite mixtures than for ferrihydrite−goethite mixtures (comparison of Figure 2e and f) reflects both the faster transformation of ferrihydrite into magnetite than goethite and the stronger pH-dependence of magnetite versus goethite reduction.
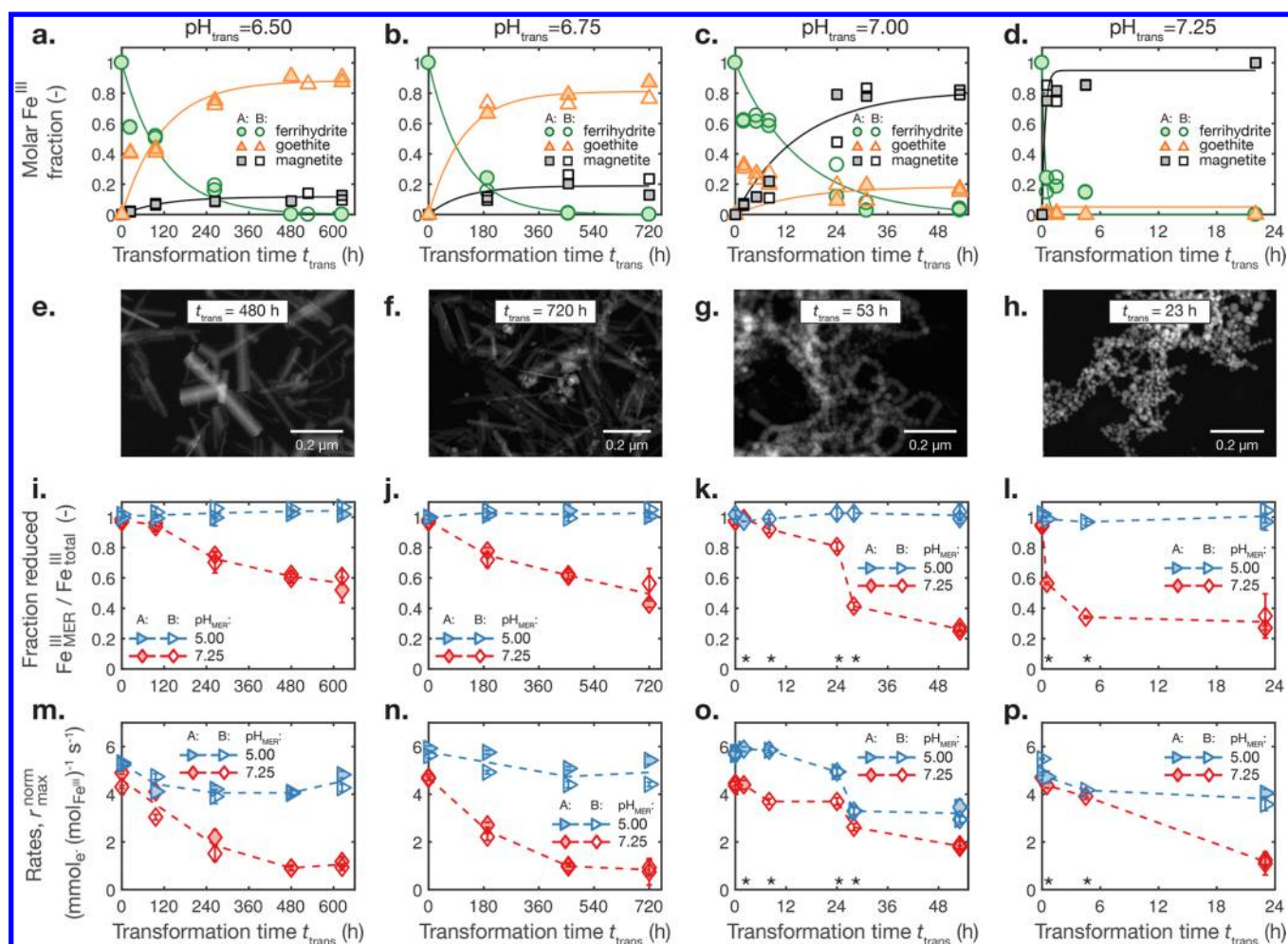
Figure 3. Changes in iron oxide mineralogy, morphology and reducibility during ferrihydrite transformation into goethite-magnetite mixtures. Transformation experiments were performed at pH_{trans} = 6.50 (a, e, i, m), 6.75 (b, f, j, n), 7.00 (c, g, k, o), and 7.25 (d, h, l, p) (all at 5 mM Fe^{2+} and 10 mM ferrihydrite-Fe^{III}). Results are shown for duplicate reactors (reactors A and B in filled and open symbols, respectively). (a−d) Changes in the molar fractions of Fe^{III} in ferrihydrite, goethite, and magnetite over the course of the transformations as determined using X-ray diffraction. Molar Fe^{III} fractions were calculated from the iron oxide mass fractions as described in Section S8.5. The mass fractions of crystalline siderite and lepidocrocite were <2.4% in all samples. Solid lines depict fitting of eqs S6−S8 to the concentrations of Fe^{III} in ferrihydrite, goethite, and magnetite (see Section S8.7). (e−h) Transmission electron microscopy images of the transformation end-products. (i−l) Changes in the fractions of oxide-Fe^{III} reduced ($Fe_{MER}^{III}/Fe_{total}^{III}$) and (m−p) normalized maximum reduction rates (r_{max}^{norm}) over the course of the transformations as quantified using mediated electrochemical reduction (MER) at pH_{MER} = 5.00 (blue triangles) and 7.25 (red diamonds) (both at applied reduction potentials of E_H^{MER} = −0.35 V). $Fe_{MER}^{III}/Fe_{total}^{III}$ and r_{max}^{norm} were determined as described in the Materials and Methods section. The dashed lines in panels i−p serve as visual guides. We note that for selected time points during the transformation experiments at pH_{trans} = 7.00 and 7.25 (marked with * on the x axes), MER data were collected for only one of the duplicate reactors because the transformation progressed too rapidly to allow for parallel MER analyses of aliquots collected from both reactors.

Overall, the results show that MER can be used to track changes in the extents and rates of iron oxide reduction over the course of mineral transformations. By spanning a range of pH_{MER} from 5.00 to 7.25, changes in iron oxide reducibility can be determined as a function of the thermodynamic boundary conditions for iron oxide reduction.

Changes in Iron Oxide Reducibility during Ferrihydrite Transformation into Both Goethite and Magnetite. *MER of Ferrihydrite−Goethite−Magnetite Mixtures.* The MER analyses discussed above were conducted on samples from transformation experiments in which ferrihydrite transformed (almost) exclusively into either goethite or magnetite. To also assess the applicability of MER to iron oxide mixtures composed of more than two minerals, we ran additional transformation experiments at pH_{trans} and Fe^{2+} conditions at which ferrihydrite is known to simultaneously

transform into both goethite and magnetite (i.e., pH_{trans} from 6.50 to 7.25, all at initial concentrations of 5 mM Fe^{2+} and 10 mM ferrihydrite-Fe^{III}). Figure 3a−d show the changes in iron oxide mineralogy over the course of the transformation experiments, as determined by XRD analyses of suspension aliquots collected from the reactors. Selected EM images of the transformation end-products are shown in Figure 3e−h (EM images collected over the course of the transformations are provided in Figures S24−S27). As we increased the pH_{trans} of the transformation experiment from 6.50 to 7.25, the amount of formed goethite decreased while that of formed magnetite increased, in line with previous studies.[23−39] As expected, the number of protons released during ferrihydrite transformation increased as the molar Fe^{III} fraction of magnetite increased (Section S12). The fitted pseudo-first order rate constants of goethite formation changed little with pH_{trans} (i.e., $k_{FH→GOE}$
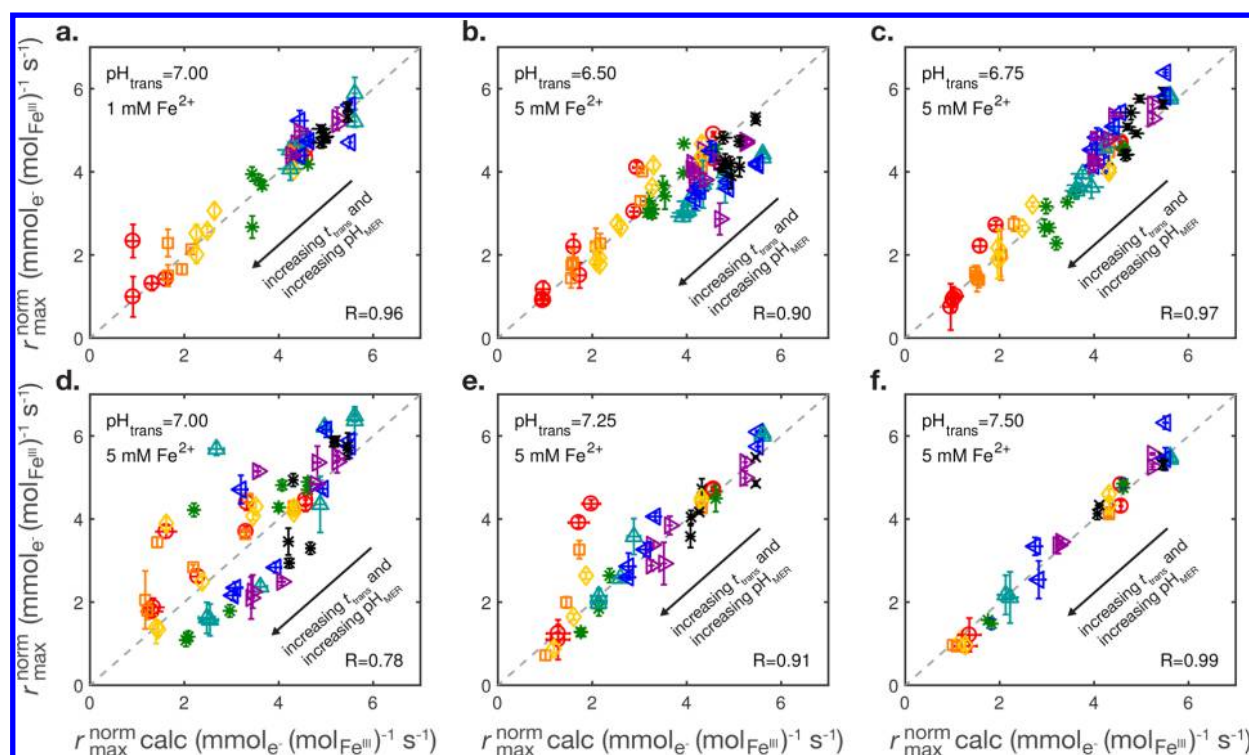
Figure 4. Link between changes in iron oxide reducibility and mineralogy. Measured values of normalized maximum iron oxide reduction rates (r_{max}^{norm}) are plotted versus values calculated based on iron oxide mineralogy (r_{max}^{norm} calc). Each panel presents data for one of the six transformation experiments (experimental conditions are reported on the plots). MER data were obtained at pH_{MER} = 5.00 (black crosses), 5.50 (purple right-pointing triangles), 6.00 (blue left-pointing triangles), 6.25 (turquois upward-pointing triangles), 6.50 (green stars), 6.75 (yellow diamonds), 7.00 (orange squares), 7.25 (red circles) (all at applied reduction potentials of E_H^{MER} = −0.35 V). Pearson correlation analysis was performed separately for each transformation experiment and correlation coefficients (R) are given on the plots (see text and Table S7 for details).

around $(90.0 \pm 19.0) \cdot 10^{-4}\ h^{-1}$). This finding was consistent with no net release of protons into solution during ferrihydrite transformation into goethite. By comparison, the rate of magnetite formation increased by more than three orders of magnitude from $k_{FH \to MAG} = (1.00 \pm 0.56) \cdot 10^{-3}\ h^{-1}$ at pH_{trans} = 6.50 to 3.05 ± 0.91 h^{-1} at pH_{trans} = 7.25 (see Section S8.7 for transformation kinetics). Ferrihydrite transformation into magnetite thus kinetically outcompeted transformation into goethite at pH_{trans} > 6.75. We note that ferrihydrite directly transformed into either goethite or magnetite at all pH_{trans} with one exception: At pH_{trans} = 7.00, a fraction of the goethite that formed within the first 2 h of Fe^{2+} addition to ferrihydrite transformed into magnetite over the course of the subsequent 51 h (Figure 3c). We did not consider this specific transformation in the kinetic modeling of the transformation data.

In analogy to the MER analyses above, we quantified changes in both the extents and maximum rates of iron oxide reduction over the course of the ferrihydrite transformations into goethite−magnetite mixtures (Figure 3i−p). At low pH_{MER} of 5.00 (E_H^{MER} = −0.35 V), the oxides in the mixtures underwent complete reductive dissolution over the course of the MER measurements, as evidenced from $Fe_{MER}^{III}/Fe_{total}^{III}$ values of ∼1 (blue triangles in Figure 3i−l). Conversely, the reduction extents of the same iron oxide mixtures at pH_{MER} = 7.25 (E_H^{MER} = −0.35 V, red diamonds) decreased over the course of the transformations reflecting formation of the crystalline oxides goethite and magnetite at the expense of poorly crystalline ferrihydrite. A comparison of panels a−d and i−l of Figure 3 also shows that the extents of iron oxide

reduction in MER decreased with increasing magnetite formation. Magnetite was the predominant transformation product of ferrihydrite at pH_{trans} = 7.25 with a final molar Fe^{III} fraction in magnetite of 0.98 ± 0.003 after 22 h (Figure 3d,h). The extents of magnetite reduction in these samples (Figure 3l) were also in good agreement with magnetite reduction extents measured at the end of the transformation experiment at pH_{trans} = 7.50 and 5 mM Fe^{2+} (Figure 2f). The changes in the maximum rates of iron oxide reduction during ferrihydrite transformations into goethite−magnetite mixtures paralleled those of the reduction extents: While maximum reduction rates at pH_{MER} = 5.00 showed no to only small decreases with increasing transformation, the maximum reduction rates at pH_{MER} = 7.25 decreased with increasing formation of goethite and magnetite (Figure 3m−p). Overall, these results highlight the capability of MER to follow changes in iron oxide reducibility during transformations that involve mixtures of three iron oxides with different crystallinities and reducibilities.

Linking Changes in Iron Oxide Reducibility and Mineralogy. We assessed if changes in iron oxide reducibility measured at different pH_{MER} over the course of the ferrihydrite transformations can be directly linked to the underlying changes in iron oxide mineralogy that we determined by XRD analysis. To this end, we used the mineralogical composition of iron oxide mixtures that we collected during the transformation experiments to calculate the reduction extents and maximum rates of these mixtures at all tested pH_{MER}. More specifically, we linearly combined the reduction extents or maximum rates of ferrihydrite, goethite and magnetite weighted by their respective molar Fe^{III} fractions in the mixture (Figures 1a,b and

3a−d). Section S15 shows the reduction extents and maximum rates of pure ferrihydrite, goethite, and magnetite, which we used in the linear combination. In the following, we discuss the agreement between measured and calculated maximum rates rather than extents of reduction because the former were more sensitive than the latter to changes in pH_{MER} and thus the thermodynamic driving force for iron oxide reduction. Yet, we draw the same conclusions if we instead compare calculated and measured reduction extents (Section S16).

Figure 4a−f show the measured versus the calculated r_{max}^{norm} for all samples collected from the six ferrihydrite transformation experiments. Each panel displays a combination of data from different stages of ferrihydrite transformation and MER measurements at various pH_{MER}. Data points in the top right corner of each panel correspond to suspension aliquots that were collected at early stages of the transformations (and therefore aliquots that predominantly contained ferrihydrite) or at later stages of the transformations but analyzed at low pH_{MER}. These data points thus had in common that they resulted from MER analyses of iron oxides with highly negative $\Delta_r G$ for iron oxide reductive dissolution. Data points shifted toward the origin with increasing transformation of ferrihydrite into goethite and magnetite and with increasing pH_{MER} at which suspension aliquots were analyzed. The $\Delta_r G$ values for iron oxide reductive dissolution thus increased to less negative values from the top right to the bottom left corners of panels a−f.

Measured and calculated r_{max}^{norm} in Figure 4a−f were in good agreement. We obtained very high Pearson correlation coefficients, R, between measured and calculated r_{max}^{norm} for suspension aliquots collected during the transformation experiments at $pH_{trans} = 7.00$ and 1 mM Fe^{2+}, $pH_{trans} = 6.75$ and 5 mM Fe^{2+}, and $pH_{trans} = 7.50$ and 5 mM Fe^{2+} (Figure 4a,c,f, $R \geq 0.97$ for all three experiments). Details on the statistical analysis are provided in Table S7. We note that we excluded the results of MER analyses of the end point suspension aliquots of the transformation experiments at $pH_{trans} = 7.00$ and 1 mM Fe^{2+} and $pH_{trans} = 7.50$ and 7.25, both at 5 mM Fe^{2+} (Figure 4a,e,f) from the correlation analyses because these data were used to determine the reducibilities of pure goethite and magnetite that we used in the calculation of r_{max}^{norm} values. The correlation between measured and calculated r_{max}^{norm} was weaker ($R = 0.78$) for suspension aliquots collected during the transformation experiment at $pH_{trans} = 7.00$ and 5 mM Fe^{2+}. We ascribe this weaker correlation to the more complex mineralogical transformation in this experiment, which included the transformation of goethite into magnetite (Figure 3c). The strong correlations between measured and calculated r_{max}^{norm} in all other experiments, however, demonstrate that we successfully linked changes in iron oxide reducibility during ferrihydrite transformation under varying thermodynamic boundary conditions for reduction to the underlying changes in iron oxide mineralogy. This outcome suggests that the thermodynamic driving force for the reduction of individual iron oxides defines the overall reducibility of oxide-Fe^{III} in iron oxide mixtures.

■ IMPLICATIONS

This work demonstrates the use of MER to quantify changes in the extents and rates of iron oxide reduction during the transformation of poorly crystalline ferrihydrite into crystalline goethite and magnetite. We show that MER is equally applicable to samples that contain one predominant iron oxide as well as mixtures of different iron oxides. In the latter case, the results of MER analyses can be explained by the additive reducibilities of the individual iron oxides weighted according to their relative molar contributions to total oxide-Fe^{III} in the sample. Finally, a given sample can be analyzed in MER over a range of thermodynamic driving forces for iron oxide reduction, implemented by systematically varying pH_{MER}, thereby offering the possibility to fine-tune the analytical conditions to the thermodynamic stabilities (i.e., E_H(oxide)) of the analyzed oxides. While we analyzed changes in iron oxide reducibility and mineralogy during ferrous iron-induced ferrihydrite transformation in this work, we propose that MER can be universally employed to study changes in iron oxide reducibility during reactions that alter the mineralogy or crystallinity (and thus the thermodynamic stability) of iron oxides. Specifically, we propose that MER can be employed to study the effect of dopants[3,28,46] and surface impurities[35,47] on changes in iron oxide reducibility during oxide phase transformations. We anticipate that the use of MER may also provide insights into longer-term changes in iron oxide reducibility in dynamic systems, including temporarily anoxic soils and sediments characterized by recurrent iron oxide dissolution and reprecipitation events.[48−50] Finally, microbial iron oxide reduction experiments may be complemented with MER analyses to determine changes in the reducibility of the iron oxides and to assess how these changes impact the extents and rates of anaerobic microbial respiration to oxide-Fe^{III}. This work introduces an analytical approach that allows to directly analyze iron oxide reducibility under defined thermodynamic boundary conditions for iron oxide reduction. We anticipate that this approach will help to elucidate the control of the electron accepting properties of iron oxides on the biogeochemical cycling of nutrients and trace metals and on the dynamics of pollutants in natural and engineered systems.

■ ASSOCIATED CONTENT

Ⓢ Supporting Information
The Supporting Information is available free of charge on the ACS Publications website at DOI: 10.1021/acs.est.8b07190.

> Chemicals used, setup of transformation experiments, ferrihydrite synthesis, pH-stat base titration curves, control ferrihydrite transformation experiment without added Fe^{2+}, iron concentrations and specific iron oxide surface areas at the end of each transformation experiment, details on XRD analysis, thermodynamics of iron oxide reduction in MER, current response during MER measurement, Matlab codes, proton release during ferrihydrite transformations, electron microscopy images, additional MER data, reducibilities of pure iron oxides, link between changes in iron oxide reduction extents and iron oxide mineralogy (PDF)

■ AUTHOR INFORMATION

Corresponding Authors
*E-mail: thomas.hofstetter@eawag.ch.
*E-mail: michael.sander@env.ethz.ch.

ORCID Ⓞ
Ralf Kaegi: 0000-0002-2430-4733
Andreas Voegelin: 0000-0003-2873-8966
Thomas B. Hofstetter: 0000-0003-1906-367X
Michael Sander: 0000-0003-3383-2041

Notes

The authors declare no competing financial interest.

■ REFERENCES

(1) Raiswell, R.; Canfield, D. E. The iron biogeochemical cycle past and present. *Geochem. perspect.* **2012**, *1*, 1−220.

(2) Taylor, K. G.; Konhauser, K. O. Iron in earth surface systems: A major player in chemical and biological processes. *Elements* **2011**, *7*, 83−88.

(3) Cornell, R. M.; Schwertmann, U. *The Iron Oxides: Structure, Properties, Reactions, Occurrences and Uses*, 2nd ed.; Second, Completely Revised and Extended ed.; Wiley-VCH Verlag: Weinheim, 2003.

(4) Deng, Y.; Stumm, W. Reactivity of aquatic iron(III) oxy-hydroxides− implications for redox cycling of iron in natural waters. *Appl. Geochem.* **1994**, *9*, 23−36.

(5) LaKind, J. S.; Stone, A. T. Reductive dissolution of goethite by phenolic reductants. *Geochim. Cosmochim. Acta* **1989**, *53*, 961−971.

(6) Peiffer, S.; Dos Santos Afonso, M.; Wehrli, B.; Gaechter, R. Kinetics and mechanism of the reaction of hydrogen sulfide with lepidocrocite. *Environ. Sci. Technol.* **1992**, *26*, 2408−2413.

(7) Rickard, D. T. Kinetics and mechanism of the sulfidation of goethite. *Am. J. Sci.* **1974**, *274*, 941−952.

(8) Roden, E. E. Microbial iron-redox cycling in subsurface environments. *Biochem. Soc. Trans.* **2012**, *40*, 1249−1256.

(9) Konhauser, K. O.; Kappler, A.; Roden, E. E. Iron in microbial metabolisms. *Elements* **2011**, *7*, 89−93.

(10) Roden, E. E. Fe(III) oxide reactivity toward biological versus chemical reduction. *Environ. Sci. Technol.* **2003**, *37*, 1319−1324.

(11) Bonneville, S.; Behrends, T.; Van Cappellen, P. Solubility and dissimilatory reduction kinetics of iron(III) oxyhydroxides: A linear free energy relationship. *Geochim. Cosmochim. Acta* **2009**, *73*, 5273−5282.

(12) Hansel, C. M.; Lentini, C. J. *Microbial Metal and Metalloid Metabolism: Advances and Applications*; Stolz, J. F., Oremland, R. S., Eds.; American Society of Microbiology Press: Washington, D.C., 2011; pp 93−115.

(13) Roden, E. E. Geochemical and microbiological controls on dissimilatory iron reduction. *C. R. Geosci.* **2006**, *338*, 456−467.

(14) Roden, E. E. Analysis of long-term bacterial vs. chemical Fe(III) oxide reduction kinetics. *Geochim. Cosmochim. Acta* **2004**, *68*, 3205−3216.

(15) Larsen, O.; Postma, D. Kinetics of reductive bulk dissolution of lepidocrocite, ferrihydrite, and goethite. *Geochim. Cosmochim. Acta* **2001**, *65*, 1367−1379.

(16) Postma, D. The reactivity of iron oxides in sediments: A kinetic approach. *Geochim. Cosmochim. Acta* **1993**, *57*, 5027−5034.

(17) Suter, D.; Banwart, S.; Stumm, W. Dissolution of hydrous iron(III) oxides by reductive mechanisms. *Langmuir* **1991**, *7*, 809−813.

(18) Dos Santos Afonso, M.; Morando, P. J.; Blesa, M. A.; Banwart, S.; Stumm, W. The reductive dissolution of iron oxides by ascorbate: The role of carboxylate anions in accelerating reductive dissolution. *J. Colloid Interface Sci.* **1990**, *138*, 74−82.

(19) Banwart, S.; Davies, S.; Stumm, W. The role of oxalate in accelerating the reductive dissolution of hematite (α-Fe$_2$O$_3$) by ascorbate. *Colloids Surf.* **1989**, *39*, 303−309.

(20) Aeppli, M.; Voegelin, A.; Gorski, C. A.; Hofstetter, T. B.; Sander, M. Mediated electrochemical reduction of iron (oxyhydr-) oxides under defined thermodynamic boundary conditions. *Environ. Sci. Technol.* **2018**, *52*, 560−570.

(21) Sander, M.; Hofstetter, T. B.; Gorski, C. A. Electrochemical analyses of redox-active iron minerals: A review of nonmediated and mediated approaches. *Environ. Sci. Technol.* **2015**, *49*, 5862−5878.

(22) Aeschbacher, M.; Sander, M.; Schwarzenbach, R. P. Novel electrochemical approach to assess the redox properties of humic substances. *Environ. Sci. Technol.* **2010**, *44*, 87−93.

(23) Xiao, W.; Jones, A. M.; Collins, R. N.; Bligh, M. W.; Waite, T. D. Use of Fourier transform infrared spectroscopy to examine the Fe(II)-catalyzed transformation of ferrihydrite. *Talanta* **2017**, *175*, 30−37.

(24) Jones, A. M.; Collins, R. N.; Waite, T. D. Redox character-ization of the Fe(II)-catalyzed transformation of ferrihydrite to goethite. *Geochim. Cosmochim. Acta* **2017**, *218*, 257−272.

(25) Dey, A.; Lenders, J. J. M.; Sommerdijk, N. A. J. M. Bioinspired magnetite formation from a disordered ferrihydrite-derived precursor. *Faraday Discuss.* **2015**, *179*, 215−225.

(26) Boland, D. D.; Collins, R. N.; Miller, C. J.; Glover, C. J.; Waite, T. D. Effect of solution and solid-phase conditions on the Fe(II)-accelerated transformation of ferrihydrite to lepidocrocite and goethite. *Environ. Sci. Technol.* **2014**, *48*, 5477−5485.

(27) Boland, D. D.; Collins, R. N.; Glover, C. J.; David Waite, T. An in situ quick-EXAFS and redox potential study of the Fe(II)-catalyzed transformation of ferrihydrite. *Colloids Surf., A* **2013**, *435*, 2−8.

(28) Hansel, C. M.; Learman, D. R.; Lentini, C. J.; Ekstrom, E. B. Effect of adsorbed and substituted Al on Fe(II)-induced mineraliza-tion pathways of ferrihydrite. *Geochim. Cosmochim. Acta* **2011**, *75*, 4653−4666.

(29) Yang, L.; Steefel, C. I.; Marcus, M. A.; Bargar, J. R. Kinetics of Fe(II)-catalyzed transformation of 6-line ferrihydrite under anaerobic flow conditions. *Environ. Sci. Technol.* **2010**, *44*, 5469−5475.

(30) Pedersen, H. D.; Postma, D.; Jakobsen, R. Release of arsenic associated with the reduction and transformation of iron oxides. *Geochim. Cosmochim. Acta* **2006**, *70*, 4116−4129.

(31) Yee, N.; Shaw, S.; Benning, L. G.; Nguyen, T. H. The rate of ferrihydrite transformation to goethite via the Fe(II) pathway. *Am. Mineral.* **2006**, *91*, 92−96.

(32) Pedersen, H. D.; Postma, D.; Jakobsen, R.; Larsen, O. Fast transformation of iron oxyhydroxides by the catalytic action of aqueous Fe(II). *Geochim. Cosmochim. Acta* **2005**, *69*, 3967−3977.

(33) Hansel, C. M.; Benner, S. G.; Fendorf, S. Competing Fe(II)-induced mineralization pathways of ferrihydrite. *Environ. Sci. Technol.* **2005**, *39*, 7147−7153.

(34) Hansel, C. M.; Benner, S. G.; Neiss, J.; Dohnalkova, A. C.; Kukkadapu, R. K.; Fendorf, S. Secondary mineralization pathways induced by dissimilatory iron reduction of ferrihydrite under advective flow. *Geochim. Cosmochim. Acta* **2003**, *67*, 2977−2992.

(35) Zachara, J. M.; Kukkadapu, R. K.; Fredrickson, J. K.; Gorby, Y. A.; Smith, S. C. Biomineralization of poorly crystalline Fe(III) oxides by dissimilatory metal reducing bacteria (DMRB). *Geomicrobiol. J.* **2002**, *19*, 179−207.

(36) Tronc, E.; Belleville, P.; Jolivet, J. P.; Livage, J. Transformation of ferric hydroxide into spinel by iron(II) adsorption. *Langmuir* **1992**, *8*, 313−319.

(37) Jolivet, J. P.; Belleville, P.; Tronc, E.; Livage, J. Influence of Fe(II) on the formation of the spinel iron oxide in alkaline medium. *Clays Clay Miner.* **1992**, *40*, 531−539.

(38) Fredrickson, J. K.; Zachara, J. M.; Kennedy, D. W.; Dong, H.; Onstott, T. C.; Hinman, N. W.; Li, S. Biogenic iron mineralization accompanying the dissimilatory reduction of hydrous ferric oxide by a groundwater bacterium. *Geochim. Cosmochim. Acta* **1998**, *62*, 3239−3257.

(39) Cornell, R. M.; Schneider, W.; Giovanoli, R. Phase trans-formations in the ferrihydrite/cysteine system. *Polyhedron* **1989**, *8*, 2829−2836.

(40) Schwertmann, U.; Cornell, R. M. *Iron Oxides in the Laboratory: Preparation and Characterization*, 2nd ed.; Second, Completely Revised and Extended Ed.; Wiley-VCH: Weinheim, 2000.

(41) Tamura, H.; Goto, K.; Yotsuyanagi, T.; Nagayama, M. Spectrophotometric determination of iron(II) with 1,10-phenanthro-

line in the presence of large amounts of iron(III). *Talanta* **1974**, *21*, 314−318.

(42) ThomasArrigo, L. K.; Byrne, J. M.; Kappler, A.; Kretzschmar, R. Impact of organic matter on iron(II)-catalyzed mineral transformations in ferrihydrite−organic matter coprecipitates. *Environ. Sci. Technol.* **2018**, *52*, 12316−12326.

(43) Scarlett, N. V. Y.; Madsen, I. C. Quantification of phases with partial or no known crystal structures. *Powder Diffr.* **2006**, *21*, 278−284.

(44) Gorski, C. A.; Scherer, M. M. Determination of nanoparticulate magnetite stoichiometry by Mössbauer spectroscopy, acidic dissolution, and powder X-ray diffraction: A critical review. *Am. Mineral.* **2010**, *95*, 1017−1026.

(45) Gorski, C. A.; Kluepfel, L. E.; Voegelin, A.; Sander, M.; Hofstetter, T. B. Redox properties of structural Fe in clay minerals. 2. Electrochemical and spectroscopic characterization of electron transfer irreversibility in ferruginous smectite, SWa-1. *Environ. Sci. Technol.* **2012**, *46*, 9369−9377.

(46) Ekstrom, E. B.; Learman, D. R.; Madden, A. S.; Hansel, C. M. Contrasting effects of Al substitution on microbial reduction of Fe(III) (hydr)oxides. *Geochim. Cosmochim. Acta* **2010**, *74*, 7086−7099.

(47) Borch, T.; Masue, Y.; Kukkadapu, R. K.; Fendorf, S. Phosphate imposed limitations on biological reduction and alteration of ferrihydrite. *Environ. Sci. Technol.* **2007**, *41*, 166−172.

(48) Ginn, B.; Meile, C.; Wilmoth, J.; Tang, Y.; Thompson, A. T. Rapid iron reduction rates are stimulated by high-amplitude redox fluctuations in a tropical forest soil. *Environ. Sci. Technol.* **2017**, *51*, 3250−3259.

(49) Thompson, A. T.; Rancourt, D. G.; Chadwick, O. A.; Chorover, J. Iron solid-phase differentiation along a redox gradient in basaltic soils. *Geochim. Cosmochim. Acta* **2011**, *75*, 119−133.

(50) Thompson, A.; Chadwick, O. A.; Rancourt, D. G.; Chorover, J. Iron-oxide crystallinity increases during soil redox oscillations. *Geochim. Cosmochim. Acta* **2006**, *70*, 1710−1727.